ELSEVIER

Earth and Planetary Science Letters 209 (2003) 361–377

EPSL

www.elsevier.com/locate/epsl

3D mechanical modeling of the GPS velocity field along the North Anatolian fault

Ann-Sophie Provost [a,*], Jean Chéry [a], Riad Hassani [b]

[a] *Laboratoire Dynamique de la Lithosphère, Université Montpellier 2, cc060, Place E. Bataillon, 34095 Montpellier Cedex 5, France*
[b] *Laboratoire d'Instrumentation Géophysique, Université de Savoie, Le Chablais, 73376 Le Bourget-du-lac, France*

Received 14 November 2002; received in revised form 17 February 2003; accepted 20 February 2003

Abstract

The North Anatolian fault (NAF) extends over 1500 km in a complex tectonic setting. In this region of the eastern Mediterranean, collision of the Arabian, African and Eurasian plates resulted in creation of mountain ranges (i.e. Zagros, Caucasus) and the westward extrusion of the Anatolian block. In this study we investigate the effects of crustal rheology on the long-term displacement rate along the NAF. Heat flow and geodetic data are used to constrain our mechanical model, built with the three-dimensional finite element code ADELI. The fault motion occurs on a material discontinuity of the model which is controlled by a Coulomb-type friction. The rheology of the lithosphere is composed of a frictional upper crust and a viscoelastic lower crust. The lithosphere is supported by a hydrostatic pressure at its base (representing the asthenospheric mantle). We model the long-term deformation of the surroundings of the NAF by adjusting the effective fault friction and also the geometry of the surface fault trace. To do so, we used a frictional range of 0.0–0.2 for the fault, and a viscosity varying between 10^{19} and 10^{21} Pa s. One of the most striking results of our rheological tests is that the upper part of the fault is locked if the friction exceeds 0.2. By comparing our results with geodetic measurements [McClusky et al., J. Geophys. Res. B 105 (2000) 5695–5719] and tectonic observations, we have defined a realistic model in which the displacement rate on the NAF reaches ~17 mm/yr for a viscosity of 10^{19} Pa s and a fault friction of 0.05. This strongly suggests that the NAF is a weak fault like the San Andreas fault in California. Adding topography with its corresponding crustal root does not induce gravity flow of Anatolia. Rather, it has the counter-intuitive effect of decreasing the westward Anatolian escape. We find a poor agreement between our calculated velocity field and what is observed with GPS in the Marmara and the Aegean regions. We suspect that the simple lithosphere model is responsible for this discrepancy. Taking into account the weaknesses of these deforming regions should allow us to build a more realistic model that would match ground observations more appropriately. On the other hand, our results fit well GPS measurements in central Anatolia, setting the basis of modeling crustal strain in Turkey.

Keywords: North Anatolian fault; mechanical modeling; finite element; fault friction; lithospheric rheology; GPS; Turkey

* Corresponding author. Tel.: +33-4-67-14-36-85; Fax: +33-4-67-52-39-08.
E-mail addresses: provost@dstu.univ-montp2.fr (A.-S. Provost), jean@dstu.univ-montp2.fr (J. Chéry), riad.hassani@univ-savoie.fr (R. Hassani).

0012-821X/03/$ – see front matter © 2003 Elsevier Science B.V. All rights reserved.
doi:10.1016/S0012-821X(03)00099-2

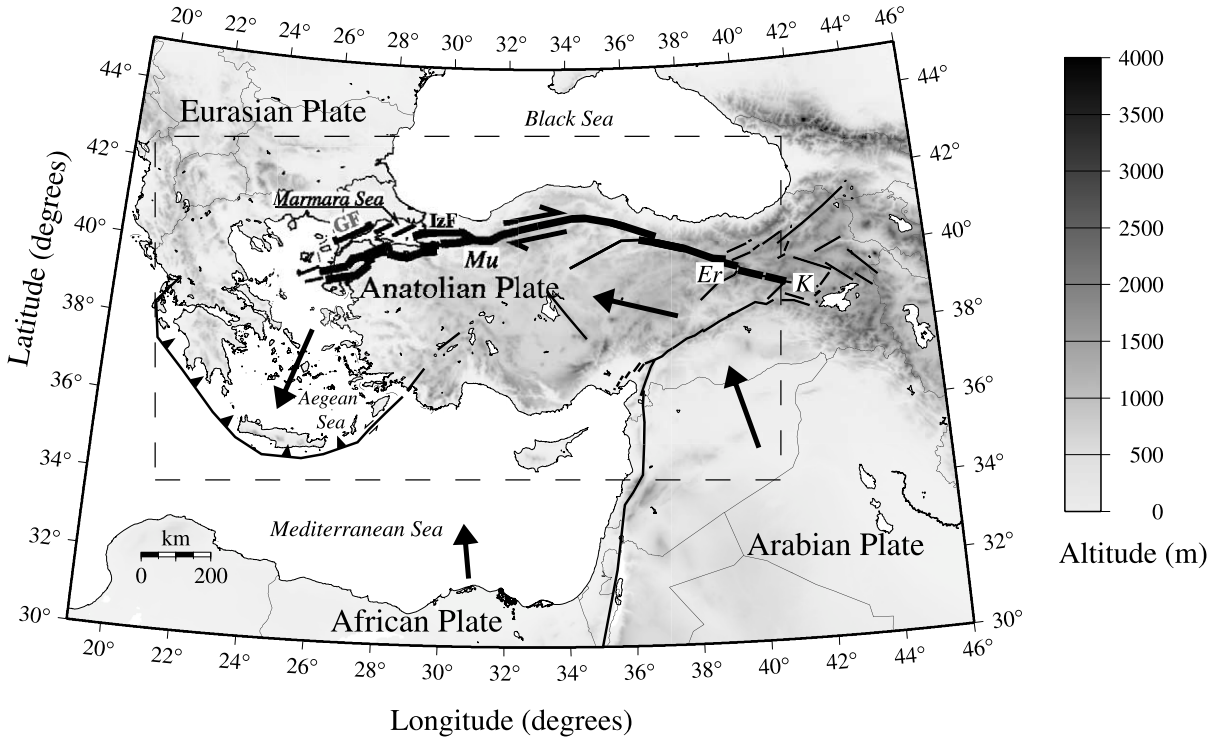

Fig. 1. Simplified tectonic map of the studied area, from the Aegean Sea to the Karliova triple junction (KTJ). The black arrows show the relative plate velocity's directions, and the thick black line shows the location of the right-lateral strike-slip NAF zone. The dashed-contour rectangle shows the boundaries of our model presented in Fig. 2. Abbreviations are: (NAF) North Anatolian fault; (K) Karliova triple junction; (Er) Erzincan; (Mu) Mudurnu Valley; (IzF) Izmit fault; (GF) Ganos fault. For this map we used the UTM projection with zone 36.

1. Introduction

The North Anatolian fault (NAF) system delineates the northern boundary of the Anatolian plate and is characterized by a right-lateral strike-slip motion [2,3]. In this complex tectonic environment the collision of the Arabian, African and Eurasian plates leads to a compressive regime to the east of the Anatolian block (creation of mountain ranges like the Zagros and the Caucasus), a right-lateral strike-slip fault zone to the north (which accommodates the westward escape of the Anatolian block [2,4]), and a subduction zone, associated with back arc spreading in the Aegean sea [2,3] to the southwestern boundary of the Anatolian block (Fig. 1). Due to the intense tectonic activity of this region, the NAF system has been the locus of large seismic events in past centuries, which presents a major risk for the population. Improving our knowledge of mechanical properties of the crust in which they take place will contribute to a better understanding of the overall tectonics of this region and the occurrence of these earthquakes. In this study we investigate the interactions between rheological properties of the Anatolian crust and the displacement rate on the NAF, constrained by heat flow and geodetic data, and using a three-dimensional (3D) mechanical model.

1.1. Velocity field in Anatolia

The NAF, as it is known today, extends over 1500 km from the Karliova triple junction (KTJ), on the east side of the Anatolian block, to mainland Greece [5] (Fig. 1). The fault mainly consists

of one strand from east to west, but when reaching the Mudurnu Valley it splits into three branches traversing the Sea of Marmara and the Aegean. Recent studies have focused on the fault geometry and tectonic evolution of the sea of Marmara region. In their analysis of the basin located between the Izmit and Ganos faults, Armijo et al. [6] have revealed no evidence for a continuous purely strike-slip fault, but rather suggest the presence of a tensional tectonic regime (pull-apart basin). However, this interpretation is not unique, and Le Pichon et al. [7] have proposed that a single, dextral strike-slip fault system cuts the entire trough. West of Marmara, the northern part of the fault system is the most active and accommodates most of the slip.

Major historical earthquakes occurred on the fault system with a westward migrating pattern, from the KTJ to the region of Marmara, in series, every 200–400 yr [8,9]. The latest one started in 1939, in eastern Turkey, with the M_w 7.9 Erzincan earthquake, rupturing the crust over 360 km and with a maximum right-lateral offset of 7.5 m. It then progressed along the fault with 10 $M > 6$ events and reached Mudurnu Valley with the recent 1999, M_w 7.4; 7.2 Izmit and Düzce earthquakes [8,10].

As a result of the accumulation of this seismic activity, the NAF system accommodates the displacement of the Anatolian plate relative to the stable Eurasian plate, at a geological rate of 16–25 mm/yr [4,5,11,12], compatible with the value of 24 ± 1 mm/yr obtained by GPS [1]. However, the total displacement on the fault system is not as homogeneous and is the subject of present controversies. According to offsets of geological features and late Miocene sediments [5] it is about 40 km near Erzincan in the east and about 25 km near Mudurnu on the west side, giving slip rates of 10 and 5 mm/yr, respectively. To constrain our model we used global velocities from GPS as the goal is not the resolve the controversies about local slip rate determination.

1.2. Heat flow

Because rock viscosity is chiefly controlled by temperature [13], knowing the heat flow density values for Anatolia's lithosphere is of great importance to constrain its rheological properties in the construction of a thermo-mechanical model. As previously mentioned, the northwestern part of Turkey marks the transition from purely strike-slip motion on the NAF to a transtensional regime in the Aegean. This region, the most seismically active part of our study zone, is associated with numerous hot springs for which the total thermal energy output adds up to 60–130 mW/m^2 [14]. This geothermal activity forms a local anomaly compared to the global heat flow of the Anatolian block. Tezcan [15] found that the heat flow density distribution of Turkey ranges from 40 to 140 mW/m^2. The highest values correspond to the very high geothermal activity in the northwest, other somewhat high values seem to be linked to metamorphic massifs and large granitic intrusions. On the other hand, no heat flow anomalies were detected near the NAF system. According to heat flow estimates deduced from silica temperature measurements [16] the crustal contribution of the heat flow density is about 50–60 mW/m^2 in the regions south of Marmara. To our knowledge, no direct heat flow measurements (i.e. borehole temperature data) have been published on central and eastern Anatolia. In the following, we consider the lithosphere as relatively hot and homogeneous. The corresponding rheological model consists of a frictional upper crust down to 15 km depth and of a ductile lower crust between 15 km and the Moho depth. We consider here that the uppermost mantle has a negligible strength compared to the crust.

2. Model

2.1. Previous work

Mechanical modeling is a key tool to infer rheological properties of the lithosphere in various regions of the globe. It has been extensively used either in two dimensions (e.g. [17–21]) or three dimensions (e.g. [22–24]). Furthermore, some researchers have focused on the complex kinematics of the eastern Mediterranean and de-

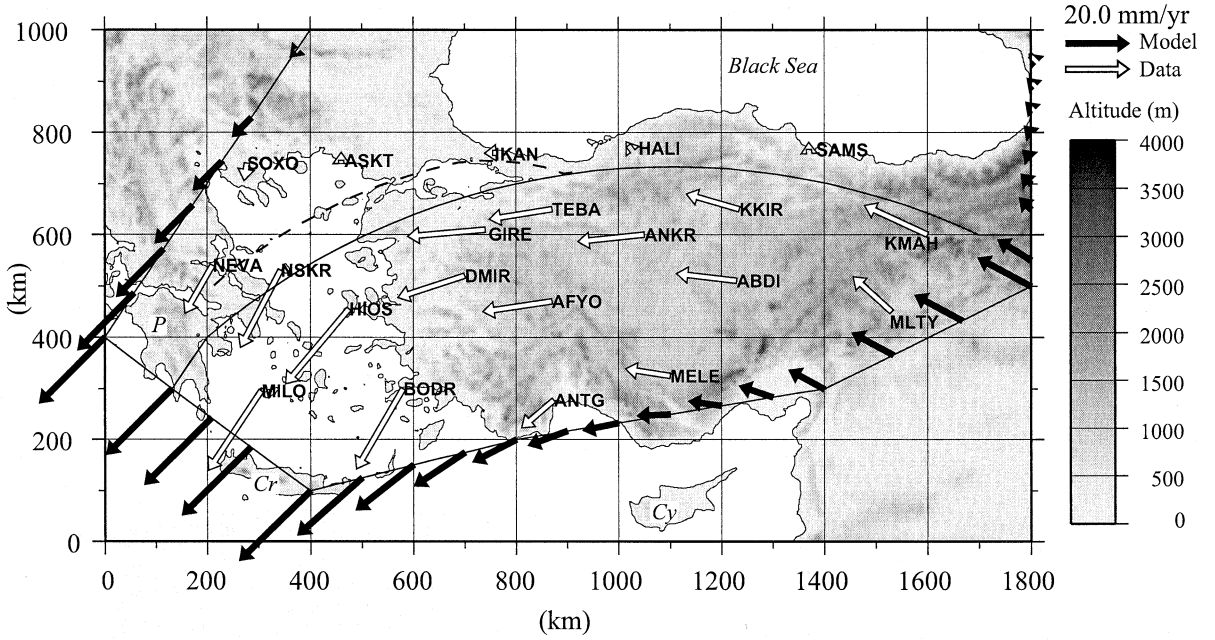

Fig. 2. Geometry of the model superimposed on the geographical map. The model extends over 1800 km and the NAF is approximated by a small circle. The dashed line represents the location of the north branch geometry used further in the experiment. The velocity boundary conditions are shown by black arrows along the faces of the model. Only the northern face is fixed, corresponding to the stable Eurasian plate. The white arrows represent the reference ground velocities deduced from GPS measurements [1], the names of the corresponding stations are plotted next to them. Abbreviations are: (P) Peloponnesus; (Cr) Crete; (Cy) Cyprus.

veloped finite element models to constrain rheological parameters of the crust in this area [25–27]. Kasapoglu and Toksoz [28] built a two-dimensional, plane stress, finite element scheme to model the interaction between the Arabian, African, Anatolian and Eurasian plates. They found that the deformation observed in the field cannot be explained by considering only a push from the Arabian and the African plates, but a supplementary driving force (gravitational push or shear forces) was necessary to produce observed movement along major faults that were modeled as relatively weak zones having a friction coefficient of 0.4–0.5. In another finite element approach, Cianetti et al. [29] found that a northward motion of Arabia at 30 mm/yr and a suction force of 40 MPa at the Hellenic trench were necessary in order to explain the velocity and stress fields observed. They also noticed that lateral variation of crustal rheology was necessary to reproduce the partitioning of the deformation from central Anatolia to central Aegean [30]. More recently, Jimenez-Munt et al. [21] have studied deformation in the whole Mediterranean and suggest that the African–Arabian vs. Eurasian collision and the subduction in the Aegean Sea are the main tectonic factors responsible for the deformation present in these regions.

Recently, extensive geodetic studies of Aegean and Anatolia have provided a precise picture of the present-day, interseismic, continental deformation [1,31]. Even if these studies do not capture the strain localization along the fault, the interseismic far field velocity is generally thought as representative of the long-term fault motion [32]. Therefore, there is a strong interest to compare the steady-state velocity field, given by 3D numerical modeling, to this dense array of velocity measurements. By doing such a comparison, we should be able to find out which rheology and fault geometry corresponds most closely to the observed velocity field.

2.2. Geometry and boundary conditions

The geometry and boundary conditions of our model have been superimposed on the topographic map of our study zone for a better visualization (Fig. 2). Our model is 1800 km long and 900 km wide (along the X and Y axes, respectively). It extends from the Peloponnesus (west) to the lesser Caucasus (east), and from the Black Sea (north) to the Island of Crete (south). We have used simple geometries for the NAF based on different models [6,7,10]. The NAF is first represented by a small circle extending from the KTJ to mainland Greece. Our crust is 30 km thick (with $\rho_c = 2800$ kg/m^3) and its base is submitted to hydrostatic forces in order to simulate the interaction with a fluid asthenosphere (with $\rho_a = 3300$ kg/m^3). We do not account for Earth sphericity and our model corresponds to a flat lithosphere. Our model is submitted to gravity forces and in a first step no initial topography is assumed. Also we did not include in this model the East Anatolian fault as our main goal is to study the strain localization along the NAF and its distribution in the fault's surroundings.

At the boundary of our model we have applied velocity gradients corresponding to horizontal velocities compiled from GPS observations [1]. Thus to simulate the plate tectonics of the area we have used horizontal velocities of $(V_x, V_y) = (-14.0, 12.5)$ mm/yr on the southeast face, corresponding to the impact of the Arabian push together with the fault slip rate of the East Anatolian fault in Eastern Anatolia. Velocities of $(V_x, V_y) = (-15.0, -25.0)$ mm/yr on the southwest face correspond to the pull of the Aegean subduction zone. The northern boundary is fixed (Eurasian plate), and the velocities on faces connecting these vary between these values (see Fig. 2). On all of the faces the vertical velocity V_z is free.

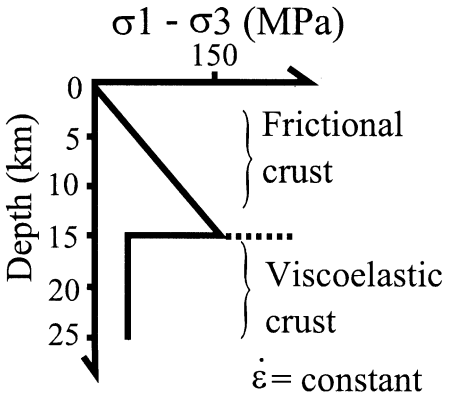

Fig. 3. Crustal rheology used in the model. See text for details.

In order to compare our results with ground observations we have used 21 reference points corresponding to GPS stations from McClusky et al. [1]. They are designated by their four-letter names and their corresponding velocity vectors are shown next to them.

2.3. Numerical formulation and constitutive laws

The crustal rheology is modeled according to pressure and temperature variations within the crust (see Fig. 3). At low P–T, the frictional crustal behavior involves a plastic yield stress that is mainly pressure-dependent. Therefore, we model the upper crust with a Drucker–Prager model [33]. We use a friction angle of 15° consistent with a high internal friction (0.6) and a hydrostatic pore pressure for the upper crust [23]. Because the frictional strain may be considered as non-dilatant at the modeled scale, we set the dilatancy angle to zero. At high P–T, a viscoelastic behavior is assumed and a linear Maxwell model is used. Although the rock viscosity is strongly temperature-dependent, we choose to use a constant viscosity for the lower crust in order to simplify the forthcoming discussion. As previously mentioned, we set the rheological change between the frictional upper crust and the viscous lower crust at 15 km depth, which is consistent with the earthquake focal depth usually observed in the Anatolian region. The NAF is represented by a small circle at the surface of the model, where the effective fault friction μ is modeled using Signorini and Coulomb laws ([18] and references therein). Therefore, the shear stress τ is limited by:

$$|\tau| = \mu_{\text{eff}} \sigma_n$$

where σ_n is the stress normal to the fault. Contact forces are computed between all nodes belonging to the discontinuity of the NAF between the sur-

face and the Moho. These forces are added to the internal and external forces in order to compute the acceleration of the mesh nodes. Velocities and displacements are computed using the dynamic relaxation method [18,34]. A mesh resolution of 20 000 elements has been used.

3. Results

3.1. Effect of friction and viscosity

In order to define a realistic rheological model we first tested the influence of viscosity and fault friction on the long-term velocity. Viscosity values between 10^{19} and 10^{21} Pa s were tested for the lower crust. To simulate a lower crust with no viscosity, we also ran numerical models where the lower crust is not involved by limiting the mesh at 15 km depth. Although this end-member case is not realistic, it allows us to evaluate the importance of the upper crustal forces and of the NAF fault friction alone. These experiments are referred to as zero-viscosity cases. Because of the lack of principal stress inversion along the NAF, it is not possible to precisely bound the effective friction of this fault as has been done on the San Andreas fault [35]. Therefore, we tested values between 0.0 (very weak fault) and 0.6 (strong fault). Fig. 4 shows the east component of the velocity difference between the IKAN and TEBA points (Fig. 2). The GPS value is 17.5 mm/yr, presumably due to the localized motion on the NAF. For lower crustal viscosities between 10^{19} and 10^{21} Pa s, the friction leading to the observed differential velocity ranges between 0.05 and 0.1. By contrast, a friction coefficient larger than 0.2 leads to velocity values lower than 6 mm/yr. A north–south velocity profile across the fault (Fig. 4b) clearly shows that the non-zero velocity difference between these two stations is not due to slip on the fault itself but rather to deformation of the crust alone. Therefore, it is possible to conclude that the fault slip rate falls to zero if the effective fault friction is larger than 0.2. The comparison with the case with zero viscosity shows that the rapid decrease of the slip rate with increasing friction is largely enhanced by the coupling of the lower crust. For example, the velocity difference is 17.5 mm/yr for the zero-viscosity case with $\mu = 0.2$, and falls to 4–6 mm/yr for other cases. We explain in Section 4 why none of the tested cases reaches the velocity of 24 mm/yr proposed by McClusky as an upper bound for the NAF velocity (see Section 4.1).

Because the coupling between the frictional part of the model and the viscous part may be dependent on the mesh size, we tested the discretization of our model and used 12 layers of elements instead of six for our 30 km thick crust. The results obtained for this case with a viscosity of 10^{19} Pa s are displayed in Fig. 4 with open diamonds. They

Table 1
Relative east–west velocities on the NAF at $x = 800$ km, $V_{naf} = (V_{TEBA} - V_{IKAN}) = 17.50$ mm/yr with McClusky's data

Case #	Model (viscosity, fault friction)	V_{naf} (mm/yr)	RMS (mm/yr)	Mean $\|\Delta V\|$ (mm/yr)	Max $\|\Delta V\|$ (mm/yr)	Name of station
1	no topo (10^{19}, 0.05)	19.80	5.06	4.28	11.78	NSKR
2	no topo (10^{19}, 0.1)	15.74	5.39	4.70	10.48	NSKR
3	no topo (10^{19}, 0.15)	8.91	6.69	6.08	11.52	HIOS
4	no topo (10^{19}, 0.2)	3.05	7.93	7.31	13.38	GIRE
5	no topo (10^{20}, 0.05)	17.44	5.27	4.52	10.81	NSKR
6	no topo (10^{21}, 0.05)	18.25	5.26	4.45	11.85	NSKR
7	no topo, no viscosity	22.33	5.31	4.22	14.35	NSKR
8	topo (10^{19}, 0.05)	16.03	5.20	4.38	8.46	ASKT
9	#8 with north branch	13.47	4.71	4.30	7.54	GIRE
10	#8 real-fault-trace	12.09	5.05	4.66	8.13	ASKT
11	#9 northwestern BC	13.96	4.54	4.14	7.44	BODR

RMS and mean $\|\Delta V\|$ between McClusky's velocity vectors and the ones estimated by our model (for 21 reference points shown in Fig. 2). The maximum value of $\|\Delta V\|$ is also mentioned along with the name of the corresponding station (see Fig. 2).

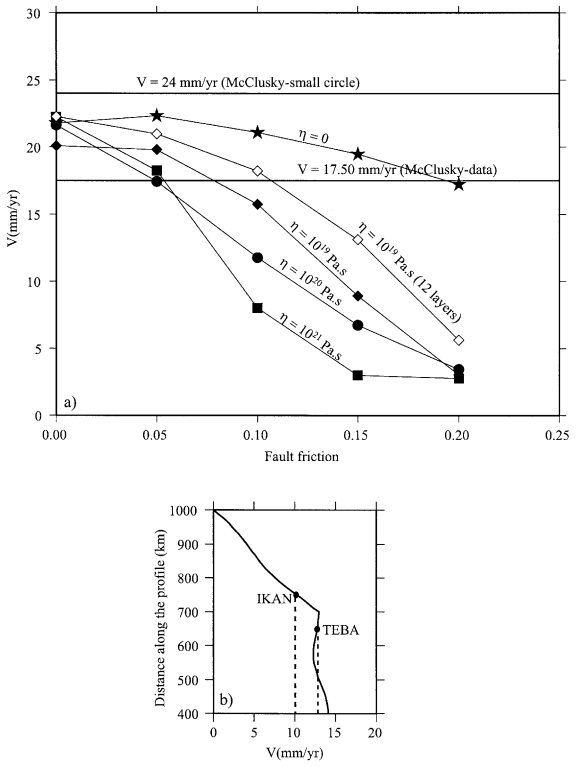

Fig. 4. (a) East component of the velocity difference between IKAN and TEBA points obtained for different viscosities and fault friction. Two reference lines were added, one at $V=17.5$ mm/yr deduced from our reference GPS measurement shown in Fig. 2 [1], and one at $V=24$ mm/yr representing the upper bound velocity across the fault [1]. (b) North–south velocity profile across the fault at $x=800$ km for case 4 with $\mu=0.2$.

slightly differ from the ones obtained with the six-layer case, with a positive offset of 2–4 mm/yr. However, they lead to the same conclusion about the effect of friction on the velocity.

According to these rheological tests, it is clear that there is a trade-off between friction and viscosity and that different couples are leading to the same differential velocity. Because a viscosity of 10^{19} Pa s for the lower crust has often been proposed as appropriate in order to model the seismic cycle (e.g. [36]), we use this value for our further experiments. Therefore the preferred friction coefficient should be 0.05 or 0.1. In order to evaluate the friction effect at the scale of Anatolia, we performed a direct comparison of our results with horizontal velocities deduced from GPS measurements [1]. We show these map views for two cases, fault friction 0.05 and 0.2 (Fig. 5a,b, respectively). Velocity vectors (black for our model and white for McClusky's GPS data) and strain rate contours are shown for both cases. A friction of 0.05 (case 1) leads to deformation concentrated in the Lesser Caucasus to the east and the Aegean region to the west, while the Anatolia does not deform. Also, the velocities of points south of the fault trace are in good agreement with the GPS data. On the other hand, relatively poor agreement occurs in the Aegean (point NSKR). Offset estimations between the data and the model are summarized in Table 1. A friction of 0.2 (case 4) leads to largely underestimated velocities for

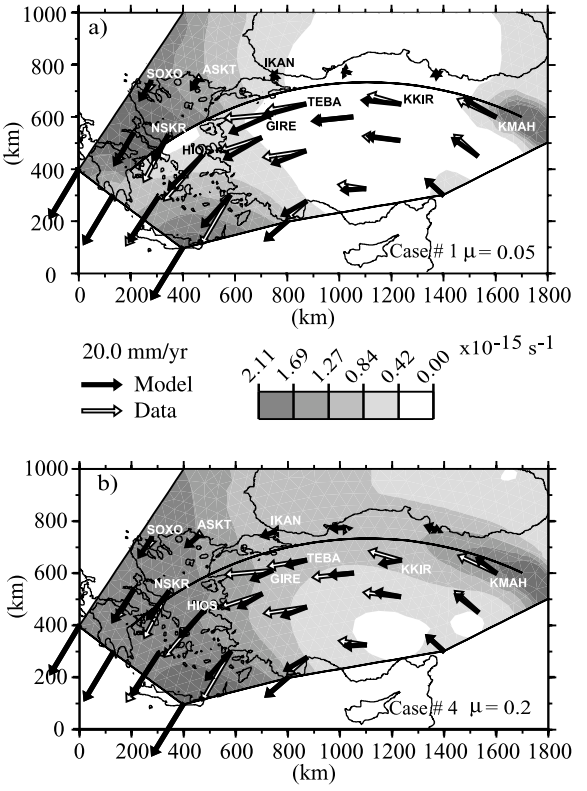

Fig. 5. Map views of the distribution of strain rate as well as velocity vectors (black arrows) deduced from the model, for two tests: fault friction of 0.05 (panel a) and 0.02 (panel b). Here the viscosity is 10^{19} Pa s. Strain rate is expressed as the quadratic invariant of the strain rate tensor. The white arrows are velocity vectors from the GPS reference points shown in Fig. 2 [1]. See text for details.

most Anatolian points (Fig. 5b), together with the low slip rate of the NAF (see Table 1). Moreover, the deformation is distributed evenly throughout the model and central Anatolia significantly deforms at a rate of 0.5×10^{-15} s^{-1}. These remarks confirm the statement, made in the last paragraph, that for a friction of 0.2 or more, our model cannot fit field observations. A preliminary conclusion is that NAF slips for only very small values of fault friction, similar to those proposed for the San Andreas fault in central California [35,37].

3.2. Effect of topography

A significant part of the crustal stress may come from differential topography [38]. Because it can affect the deformation field, we performed a numerical experiment including topography (for a viscosity of 10^{19} Pa s and a friction of 0.05, case 8). Our model contains only the long-wavelength part of the topography as shown in Fig. 6a. A crustal root which isostatically compensates the topography is assumed according to crustal and mantle density. Therefore the minimum crustal thickness is in the Aegean and Black seas (24 km) and the maximum appears in the Lesser Caucasus (44 km). In order to check the effect of the topography separately from the effect of lateral-velocity boundary conditions, we first ran a model where all velocity boundary conditions were set to zero, (i.e. no displacement occurs on the model boundaries). The differential topography induces a transient gravitational flow, which progressively decreases and finally ceases. The surface velocity goes to zero. The corresponding displacement field has an orientation perpendicular to the topographic contours (Fig. 6a). The maximum amplitude of this gravitational motion is ~200 m, which occurs between the eastern Anatolian plateau and the Black Sea where the differential topography is the highest. We then ran a model including the lateral boundary conditions as in case 1, but with topography (case 8), and we compared the results with the ones previously obtained in case 1. For this case, and the following ones, a short transient phase due to topographic loading is followed by a long enough stationary

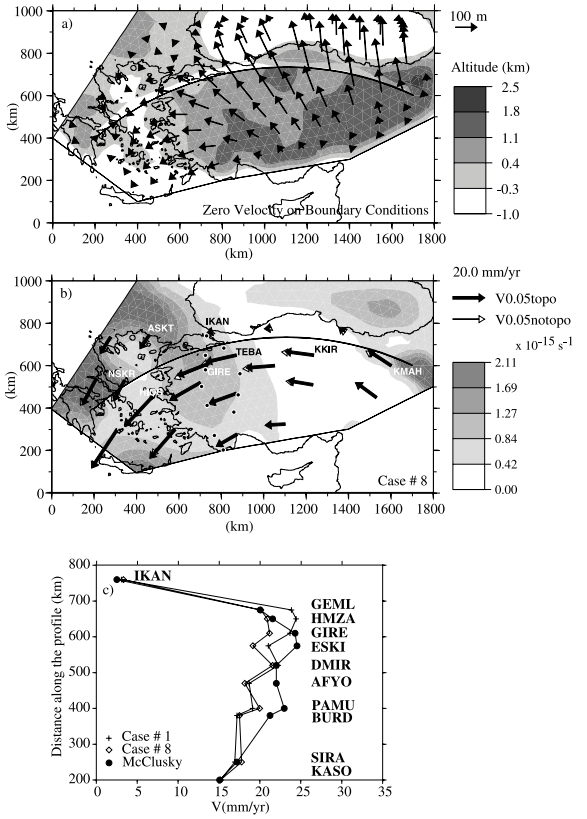

Fig. 6. Comparison of cases 1 and 8, no topography vs. topography. (a) Displacement vectors (m) due to the sole effect of topography (km) on our model. (b) Velocity vectors for case 1, without topography (white arrows) and case 8, with topography (black arrows) superimposed on the deformation distribution calculated for case 8. Small black circles show the reference points used to make the profile in panel c. (c) Profile across the fault, at $x=800$ km, of the long-term velocity resulting from the two cases mentioned above, with (open diamonds) and without (plusses) topography. Here we used a fault friction of 0.05 and a viscosity of 10^{19} Pa s. The reference line [1] is highlighted by closed circles.

phase so that the contribution of the transient phase to total displacement is very small. Fig. 6b displays the final velocity for the two experiments. The added topography has little effect on the velocity pattern. The overall effect is to decrease the velocity of 2–4 mm/yr on the sites south of the NAF (GIRE, TEBA, KKIR, KMAH). By contrast, the ASKT velocity (northern Greece) increases by 4 mm/yr. The velocity changes can be more precisely evaluated on three profiles (Fig.

6c); one for the case without topography (case 1, crosses), one with topography (case 8, open diamonds) and one estimated from McClusky's velocity vectors (closed circles) [1]. Our profiles were computed starting at $(x,y)=(800,200)$ km (see Fig. 2) over 600 km northward and correspond to the points AFYO, DMIR, GIRE, IKAN, and the points shown as solid circles in Fig. 6b. The two solutions given by cases 1 and 8 underestimate the velocity of Anatolia by about 1–5 mm/yr. A difference between the two cases (1 and 8) only occurs south of the fault. The velocity change between GIRE and IKAN is 19.8 mm/yr for the case without topography, and 16 mm/yr for the case with topography (see Table 1). Because the velocity fields of the cases 1 and 8 are roughly similar, and because the meshes related to these two cases have different discretizations, one may ask if the difference has a numerical origin. In an attempt to answer this question, we computed the solutions of 12-layer models, for cases 1 and 8. Because a trend similar to the one observed for the six-layer models is observed, we conclude that the reduced motion observed in case 8 is not a numerical artifact.

Therefore, our modeling predicts a decreasing velocity of northern Anatolia when gravitational forces of the topography are included. At first glance, this behavior seems puzzling because body forces induce a northwest directed motion associated with the topographic gradient (Fig. 6a). This effect should therefore increase the westward Anatolian velocity. However, we recall that the long-term velocity due to the gravitational effect alone goes to zero. This means that the generated differential stresses do not overcome the strength of the Anatolian lithosphere. Thus, the simple idea that topography induces lithospheric flow, as has been proposed by numerous authors [39,40], is not supported by our modeling. Nevertheless, it still remains puzzling that when topographic forces are included, the escape of the Anatolian plateau is slowed down. We think that this behavior is directly linked to the Coulomb law used to control the NAF shear stress. Indeed, the shear stress scales with μ and σ_n. Because the weight of Anatolian topography on the sides of the NAF fault increases its normal stress by several MPa, this makes the fault plane a little more resistant and less prone to slide.

3.3. Effect of geometry and boundary conditions

Considering the complex geometry of the western part of the NAF compared to the eastern NAF (see Fig. 1), we tested two new fault geometries to see their influence on stress and strain in Anatolia. The first geometry concerns the region of the Sea of Marmara where the NAF splits into three branches, with one more north than the others. In this area, GPS and geological information suggest that the north NAF is more active than the south branch [1,6,41,42]. We thus designed the western portion of the fault so that it would match the trace of the north branch in this area (case 9, see Fig. 7a for a map view). This geometrical change has a clear effect on the western and northern parts of the model. The region which corresponds to northern Greece deforms significantly. This does not seem to be consistent with the motion at the SOXO and ASKT sites. Also, a deforming zone is present 300 km southwest of the Marmara region, indicating that Anatolia does not behave rigidly there. This is consistent with observations of McClusky et al. [1] that show considerable strain in western Turkey. One can also notice that the region of the Sea of Marmara, which has been described as an actively deforming pull-apart basin [6], does not suffer a large deformation in our model. A positive consequence of this change of fault geometry is that velocities in the Aegean are more consistent with GPS motions, e.g. for the NSKR site. Overall, the north branch case seems more satisfactory and indicates that the fully circular approximation made for the NAF for cases 1–8 causes a significant deformation mismatch in the Aegean.

The second geometry fits as closely as possible the real trace of the fault from the KTJ to the Aegean Sea (case 10, see Fig. 7b for a map view). It is composed of five connected segments, all with the same fault friction of 0.05 (Table 1). The deformation distribution on the Anatolian block is not very different from that for the previous case. The most noticeable difference occurs south of the sharp NAF bend in central Anatolia

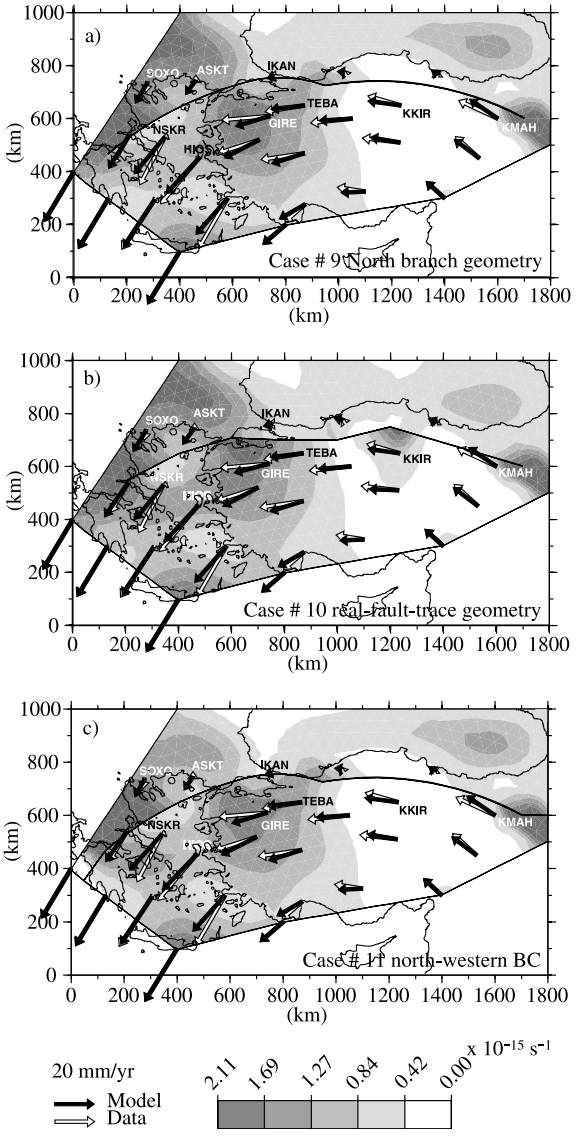

Fig. 7. Map views of the distribution of the deformation as well as velocity vectors (black arrows) deduced from the model, for two geometrical tests: northern branch geometry in the region of Marmara (case 9; panel a) and the real fault trace geometry over the whole of Anatolia (case 10; panel b), and for a boundary condition test: northern Greece boundary condition changed (case 11; panel c). The white arrows are velocity vectors from the GPS reference points shown in Fig. 2 [1]. See text for details.

(at $x = 1200$ km), where the strain rate reaches 2×10^{-15} s^{-1}. However, it must be pointed out that the motion of the corresponding GPS site KKIR is not significantly affected by the bend. As for case 9, the velocity of points of northern Greece is overestimated by 5–8 mm/yr.

A possible cause of the mismatch of the modeled velocities in northern Greece is tied to the western boundary condition of the model. Indeed, we simply impose a linear variation from zero velocity (Eurasia) to 30 mm/yr to the southwest (south Peloponnesus). Detailed GPS and tectonic studies in Greece have demonstrated that a large part of extensive strain is concentrated within the Corinth Gulf (14 mm/yr in its western part) and within the adjacent part of continental Greece. To account for this strain localization, the northwestern boundary of our case 11 was changed to fit the non-deforming northern Greece one and a localized velocity gradient of 15 mm/yr around the Corinth Gulf (Fig. 7c). As a result, the deformation remains unchanged in most parts of the model with respect to case 9, with a significant decrease in the northwestern part only. Velocities at stations SOXO and ASKT are reduced by 30% compared to the ones in case 9, without reaching the observed values.

4. Discussion

None of the 10 numerical experiments summarized in Table 1 provides very good agreement with the GPS velocity field. The RMS errors between the 21 inner control points vary from 7.93 mm/yr for case 4 ($\mu = 0.2$) to 4.71 mm/yr for case 9 (the north branch, $\mu = 0.05$), supporting our choice of 0.05 for fault friction. This result is consistent with the early work of Kasapoglu and Toksöz [28] that found the NAF is locked with a friction coefficient of 0.4. This is also in close agreement with the thin-shell finite element tectonic model of the whole Mediterranean proposed by Jimenez-Munt and Sabadini [43]. Their predictions revealed that a very low friction (0.05) is necessary on the NAF to observe the Anatolian block rotation illustrated by GPS measurements. On the other hand, their results favor a hard lith-

ospheric rheology, while according to their computations we use a soft or medium rheology in our model.

Concerning the fault geometry, the north branch cases (9 and 11), and to a lesser extent the real fault trace case (10), display better agreement with velocity data than the other cases. We now evaluate in more detail how our models match the long-term slip rate of the NAF and how the predicted stress field fits with available stress data in Anatolia.

4.1. Fault slip rate of the NAF

A good measure of the quality of these models is provided by the fault slip rate of the NAF, which can be assessed by geodetic and geological measurements. The east velocity difference between TEBA and IKAN is 17.5 mm/yr and provides an estimate of the NAF velocity (Table 1). This value is significantly smaller than the value of 24 mm/yr proposed by McClusky et al. [1] when considering that Anatolia rotates rigidly relative to Eurasia around a pole located near the Sinai. The reason for this discrepancy is the progressive decrease of the site velocities when approaching the fault. Indeed, the sites that are within 100 km south of the fault (GIRE, HMZA, GEML; see Fig. 6c) see their velocity decreasing from 24 to 19 mm/yr with increasing latitude. This velocity decrease can be interpreted in two ways. First, this may correspond to a permanent deformation of the crust by wrenching in the NAF vicinity. To our knowledge this has not been directly documented. However, it is remarkable that long-term slip rates given by geological studies [11] are systematically smaller than 24 mm/yr. Another hypothesis is that velocity decrease may correspond to an interseismic transient, i.e. the elastic strain accumulation during the seismic cycle, as suggested by McClusky et al. [1]. Indeed, large earthquakes ($M > 7$) occurred on the whole length of the NAF during the 20th century and a post-seismic effect may still occur away from the fault [44–46]. Therefore, the velocity of GPS sites within 100 km of the fault may not be representative of the long-term velocity.

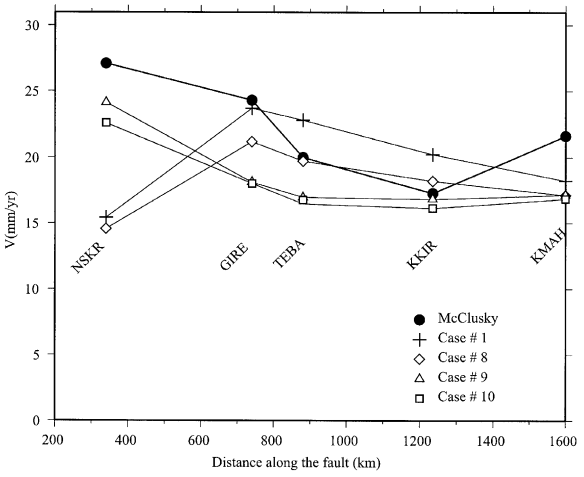

Fig. 8. Velocities at five reference points along the fault, NSKR GIRE TEBA KKIR and KMAH, for various experiments: without topography (case 1; plusses), with topography (case 8; open diamonds), with the new branch to the north (case 9; open triangles), and with the real fault trace geometry (case 10; open squares). McClusky's [1] reference line is represented by closed circles.

In order to precisely evaluate the data–model agreement around the NAF, we compare the GPS site velocities of five sites in Anatolia and Greece (Fig. 8) with the velocities predicted for cases 1, 8, 9, and 10. Because GPS sites north of the fault move slightly to the west (0–4 mm/yr), the values of Fig. 8 represent an upper bound of the differential velocity between Anatolia and Eurasia. However, the data reflect that the Anatolian motion and probably the NAF slip rate are not constant with distance along the fault. The GPS velocity is 22 mm/yr to the east (KMAH), decreases to 17 mm/yr in central Anatolia (KKIR), then increases to 20, 24 and 27 mm/yr (TEBA, GIRE and NSKR, respectively). We acknowledge that the velocity differences along the fault could also be due to other factors, such as distance from the fault or fault branches. Nevertheless, it is significant that cases 1 and 8 completely fail to mimic the NSKR motion (15 mm/yr). This is clearly due to the position of the western end of our fault, which is east of this point. Cases 9 and 10, which are geometrically more realistic, predict velocities of 24 and 23 mm/yr, respectively.

All the models fail to reproduce the velocity transition observed south of the Marmara region. The predicted velocity of GIRE and TEBA is underestimated by 4–8 mm/yr for cases 9 and 10. These low velocities are probably due to the bend associated to these cases. Indeed, cases 9 and 10 force the slip to be restricted to the north NAF only. In nature, the deformation of the Marmara zone is accommodated by different faults (north Marmara fault system, south NAF), which probably allow an easier accommodation of the motion between Anatolia and Eurasia. It has been proposed that most of this motion occurs on the north NAF, while no more than 20% occurs on the south NAF [6,42]. We are not reaching this level of complexity here, but it can be conjectured that the introduction of the different NAF strands and of the deformable Marmara region, in the model, could allow a better fit of neighboring GPS site velocities. Using a dislocation model in an elastic half-space, Flerit et al. [47] built an interseismic model of the Marmara pull-apart. They started with a one-branch fault geometry for the NAF west of Marmara and then added more complexity to the model with two branches for the NAF and extensional structures in western Turkey. Even though the velocity vectors computed by their model have amplitudes similar to the GPS ones, their azimuths differ by 11–18°, especially in the region just south of the sea of Marmara (site GIRE). According to this, even using a specific fault geometry for this region does not allow one to reproduce the velocity field deduced from GPS measurements. It would probably be necessary to introduce a weak rheology in the Marmara trough or in western Turkey to localize the deformation and reduce the thickness of the crust in this area.

Central Anatolia motion given by KKIR is well modeled by cases 8–10. To the east the KMAH velocity is systematically underestimated by 4 mm/yr. This low value is clearly due to the termination of the fault in our model at $x = 1700$ km. This induces a deformation zone around the fault tip that reaches the point KMAH and decreases its velocity. Modeling the KTJ with a slipping fault to the east should improve the velocity fit and correct this model artifact.

4.2. Stress field in Anatolia and Aegean

4.2.1. Stress data

In order to compare the stress results obtained with our model with known stress regimes in Anatolia we have collected stress data from the literature. We have superimposed the results on stress regimes and orientation maps calculated with our models (Fig. 9). White arrows represent these data, while black ones represent our results.

In general, slip on the NAF is dominated by right-lateral strike-slip motion, but some thrusting is detected east of KTJ after the intersection with the East Anatolian fault, and some normal faulting is present on the western end of the fault system before it connects with the Aegean [48]. P and T axes deduced from fault-plane solutions of major earthquakes on the central NAF show compression oriented at about 50° from the trace of major faults in a mostly right-lateral strike-slip regime, while further to the east, near the KTJ, fault-plane solutions show some thrusting component associated with right-lateral strike-slip [48]. Some evidence of active thrust faulting, away from the fault, at the southern Black Sea margin was revealed by the M_w 6.6 Bartin earthquake of 1968 [49]. Several small to moderate events have occurred in this area, and most of them show a reverse fault-plane solution with one of their nodal planes roughly parallel to the margin. This indicates the presence of compressional stresses oriented approximately perpendicular to the margin. In central western Anatolia, Zanchi and Angelier [50] were able to invert about 66 fault-plane solutions and obtained a stress tensor showing a NNE–SSW extension, with the azimuth of the least principal stress σ_3 at N25°E. In the Sea of Marmara area, geological evidence has been interpreted as a combination of strike-slip and normal faults [6]. Compilation of stress data [51] shows a north–south extension in the northwestern part of the Aegean and Anatolia with S_H (maximum horizontal compression) oriented N85°E. In the region of the Marmara Sea stress data show a more heterogeneous stress field, corresponding to the transition to a purely strike-slip regime in central Anatolia [51].

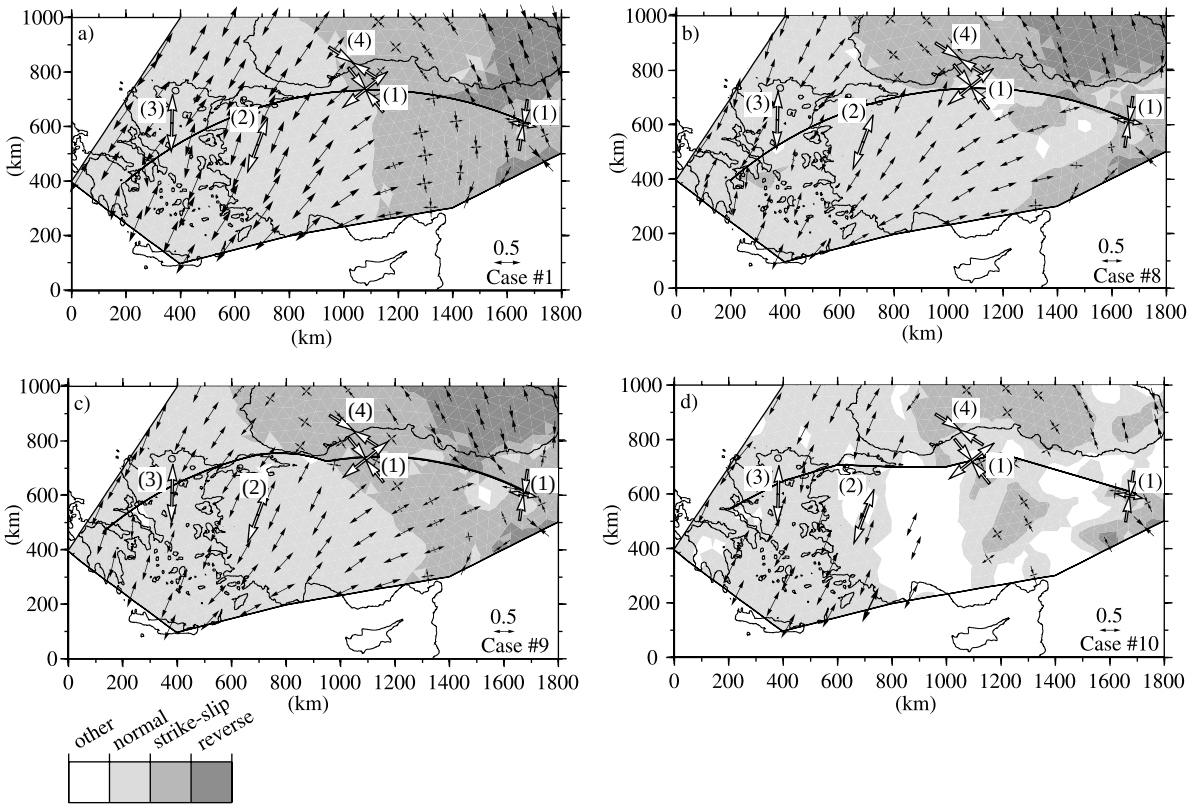

Fig. 9. Map views of the stress regimes and orientations deduced from the model for four cases, without topography (a), with topography (b), with the new branch to the north (c), and with the real fault trace geometry (d). Black arrows represent the results obtained with our modeling, their length scales with $(\sigma_1-\sigma_3)/\overline{\sigma}$, while white arrows refer to data taken from the literature: (1) [48], (2) [50], (3) [51], and (4) [49]. For a better viewing the white arrows were enlarged, the scale does not apply for these data. See text for details.

4.2.2. Stress model

Stress orientation and stress regime distributions of the four cases 1, 8, 9 and 10 are represented in Fig. 9. This stress map has been drawn at a mean depth of 7 km, and is representative of the state of deviatoric stress in the seismogenic crust with the orientation of minimum and maximum horizontal stress. The amplitudes of the orientations are based on the following ratio: $\sigma_1-\sigma_3/\overline{\sigma}$, where σ_1 and σ_3 are the absolute magnitude of the maximum and least principal stresses, respectively, and $\overline{\sigma}$ is the mean stress. We emphasize that these values do not provide any information on the strain rate which has been previously discussed. The three tectonic states of stress are present on this map. The overall picture given by cases 1, 8, 9 and 10 is an extensional domain to the west (Aegean and western Anatolia), a strike-slip domain (Black sea and eastern Anatolia) and a compressional domain to the east (Caucasus). This is in agreement with the data collected and mentioned above, showing the presence of normal faults in the Aegean [51], mostly right-lateral strike-slip earthquakes along the NAF [48], and a strong thrust component in the fault-plane solutions of events occurring in the East [48]. In our model this pattern is mainly due to the lateral boundary conditions that evolve from compressive to extensional between east and west. Most of the differences between the four cases occur in central Anatolia. For example, the normal to strike-slip transition occurs at $x=1100$ km for case 1 (no topography). On the other hand, the extensional domain invades the

whole Anatolian plateau for case 8 (with topography). This change is easily understandable, as a high plateau can be under extension due to its own weight [38]. However, not only lateral boundary conditions and topographic weight are responsible for the stress state: the normal to strike-slip limit in case 9 (north branch case) moves to the west, due to the deviation of the NAF. Unfortunately, the differences observed between these four cases mainly occur in central Anatolia, where the seismic strain is very low, i.e. smaller than 10^{-15} s^{-1} for $\mu = 0.05$, which is in agreement with observations and data (see Figs. 5–7). It is therefore difficult to discriminate among these models on the base of stress data. The GPS-based velocity field and the geological slip rate of the NAF provide better constraints on the mechanical behavior of the Aegean–Anatolian system.

4.3. Cause for disparity between model and data

Most of the discrepancy between GPS velocities and those predicted by our models occurs in the western part of the model (Greece and western Anatolia). If we choose cases 9–11 (north branch and real fault trace; see Fig. 7) for the purpose of discussion, three zones of the model do not provide a good fit to the GPS velocities.

The first zone is the Marmara region. The site GIRE has a velocity underestimated by 7.5 mm/yr. It is probable that adding the south branch of the NAF, as well as east–west grabens in western Turkey highlighted by historical seismicity, would lead to a velocity gain for the GIRE site.

The second zone is the Aegean (NSKR, HIOS, BODR and MILO). Only MILO, which is close to the boundary condition imposed along the Crete island, has a correct velocity. The other three sites have velocities underestimated by about 5 mm/yr. Therefore, a N40° extension Aegean is predicted at 5 mm/yr, in disagreement with GPS data, which do not show a significant deformation. Different causes can be responsible for such a discrepancy: (1) the Aegean lithosphere is more rigid than expected in the model; (2) a viscous flow with a N220° direction at the base of the lithosphere forces the Aegean crust to move southwest; (3) the ill-modeled adjacent zones of Marmara and western Turkey have an impact on the motion of the Aegean.

The third zone is northern Greece (SOXO and ASKT). Case 9 displays a velocity of 8 mm/yr for these two sites. Corresponding GPS velocities do not exceed 3 mm/yr. In this area, the cause for such a misfit is the lack of deformation occurring in active grabens such as the Corinth Gulf, the Evvia graben and the North Aegean trough. For example, the Corinth Gulf is opening at a rate of 11–14 mm/yr in a narrow zone of 15 km [31]. The continent north of the gulf is not deformed. On the contrary, our model shows that northern Greece deforms rather homogeneously, and active deformation reaches the northwest corner of the model. This is clearly due to the northwest boundary condition of our model, which imposes a linearly decreasing viscosity from southwest to northeast on the edge. Modifying this boundary condition, as is done in case 11, reduces the velocities of the two GPS stations considered and localizes the deformation in the region of the grabens. Thus modeling the Corinth Gulf as a strain localization zone is needed to reproduce the velocity pattern of northern Greece.

5. Conclusion

Our numerical modeling of the Anatolian plateau allowed us to integrate the forces acting on the lithospheric system in terms of velocity boundary conditions and body forces due to the topography. According to borehole stress data and rock mechanics experiments (i.e. an effective friction of 0.6), we made the assumption that the lithospheric crust can sustain a high stress. Under this condition, our numerical modeling indicates that the NAF must be a very weak material heterogeneity of the lithosphere. Indeed, we need to assign a very low effective friction on the NAF (0.05) to reproduce the first-order character of the velocity field. Because the velocity field around and inside the Anatolian plateau is well known, the modeling is accurate enough to predict that the upper bound of the effective friction should not be higher than 0.1. This value is sim-

ilar to that proposed for the SAF using stress data [35,37,52]. The effective fault velocity is here revealed using GPS velocity data alone. Stress data appear here as a secondary data set that do not contradict the conclusion previously drawn. Used in conjunction with dense GPS data, 3D numerical modeling appears to be an efficient tool to constrain the rheological properties of the lithosphere. However, the present study displays intriguing discrepancies between modeled velocities with respect to the GPS. This probably means that some limitations of the present study need to be tackled in order to step beyond. The main one is that the lithosphere is not homogeneous. A more accurate modeling should therefore account for the lateral strength variations across the eastern Mediterranean as well as the presence of the uppermost mantle as a mechanical layer. A second problem relies on the systematic use of the kinematically prescribed boundary conditions (velocities), which overlooks the lithospheric system. The use of a stress boundary condition on the southern part of the Aegean and Anatolia would allow one to reproduce more closely the true effect of the African subduction. Adding such a degree of freedom could also lead to a better evaluation of the impact of the differential topography on the predicted velocity field.

Acknowledgements

We are grateful to the reviewers Peter Bird and Robert Reilinger whose helpful comments substantially improved the manuscript. This work has been supported by the research program 'ACI Prévention des catastrophes naturelles' of the French Ministry of Research.*[AC]*

References

[1] S. McClusky, S. Balassanian, A.A. Barka, C. Demir, S. Ergintav, I. Georgiev, O. Gurkan, M. Hamburger, K. Hurst, H. Kahle, K. Kastens, G. Kekelidze, R. King, V. Kotzev, O. Lenk, S. Mahmoud, M. Nadariya, A. Ouzounis, D. Paradissis, Y. Peter, M. Prilepin, R. Reilinger, I. Sanli, H. Seeger, A. Tealeb, M.N. Toksoz, G. Veis, Global positioning system constraints on plate kinematics and dynamics in the eastern mediterranean and Caucasus, J. Geophys. Res. 105 (2000) 5695–5719.

[2] D. McKenzie, Active tectonics of the Mediterranean region, Geophys. J. R. Astron. Soc. 30 (1972) 109–185.

[3] A.A. Barka, L. Gülen, New contraints on age and total offset of the North Anatolian fault zone: implications for tectonics of the Eastern Mediterranean region, in: Melih Tokay Symposium, Spec. Publ. Middel-east Techn. Univ., Ankara, 1988, pp. 39–65.

[4] A.M.C. Sengör, The North Anatolian transform fault its age, offset and tectonic significance, J. Geol. Soc. London 136 (1979) 269–282.

[5] A.A. Barka, The North Anatolian fault zone, Ann. Tecton. VI (Special Issue) (1992) 164–195.

[6] R. Armijo, B. Meyer, S. Navarro, G. King, A.A. Barka, Asymmetric slip partitioning in the Sea of Marmara pull-apart: a clue to propagation processes of the North Anatolian fault?, Terra Nova 14 (2002) 80–86.

[7] X. Le Pichon, A.M.C. Sengör, E. Demirbag, C. Rangin, C. Imren, R. Armijo, N. Gorur, N. Cagatay, B. Mercier de Lepinay, B. Meyer, R. Saatçilar, B. Tok, The active main Marmara fault, Earth Planet. Sci. Lett. 192 (2001) 595–616.

[8] A.A. Barka, Slip distribution along the North Anatolian fault associated with the large earthquakes of the period 1939 to 1967, Bull. Seismol. Soc. Am. 86 (1996) 1238–1254.

[9] N.N. Ambraseys, The seismic activity of the Marmara sea region over the last 2000 years, Bull. Seismol. Soc. Am. 92 (2002) 1–18.

[10] A.A. Barka, H.S. Akyüz, E. Altunnel, G. Sunal, Z. Cakir, A. Dikbas, B. Yerli, R. Armijo, B. Meyer, J.B. de Chabalier, T. Rockwell, J.R. Dolan, R. Hartleb, T. Dawson, S. Christofferson, A. Tucker, T. Fumal, R. Langridge, H. Stenner, W. Lettis, J. Bachhuber, W. Page, The surface rupture and slip distribution of the 17 August 1999 Izmit earthquake (M 7.4), North Anatolian Fault, Bull. Seismol. Soc. Am. 92 (2002) 43–60.

[11] R. Armijo, B. Meyer, A. Hubert, A.A. Barka, Westward propagation of the North Anatolian fault into the northern Aegean: Timing and kinematics, Geology 27 (1999) 267–270.

[12] R. Westaway, Present-day kinematics of the Middle East and eastern Mediterranean, J. Geophys. Res. 99 (1994) 12,071–12,090.

[13] S.H. Kirby, A.K. Kronenberg, Rheology of the lithosphere: selected topics, Rev. Geophys. 25 (1987) 1219–1244.

[14] M. Pfister, L. Rybach, S. Simsek, Geothermal reconnaissance of the Marmara Sea region (NW Turkey): surface heat flow density in an area of active continental extension, Tectonophysics 291 (1998) 77–89.

[15] A.K. Tezcan, Geothermal explorations and heat flow in Turkey, in: M. Yamano (Ed.), Terrestrial Heat Flow and Geothermal Energy in Asia, A.A. Balkema, Rotterdam, 1995, pp. 23–42.

[16] M.O. Ilkisik, Regional heat flow in western Anatolian using silica temperature estimates from thermal springs, Tectonophysics 244 (1995) 175–184.
[17] P. Bird, J. Baumgardner, Fault friction, regional stress, and crust-mantle coupling in souther California from finite element methods, J. Geophys. Res. 89 (1984) 1932–1944.
[18] R. Hassani, D. Jongmans, J. Chéry, Study of plate deformation and stress in subduction processes using two-dimensional numerical models, J. Geophys. Res. 102 (1997) 17951–17965.
[19] P. Bird, Testing hypothese on plate-driving mechanisms with global lithosphere models including, topography, thermal structure, and faults, J. Geophys. Res. 103 (1998) 10115–10129.
[20] M. Roy, L.H. Royden, Crustal rheology and faulting at strike-slip boundaries 2. Effects of lower crustal flow, J. Geophys. Res. 105 (2000) 5599–5613.
[21] I. Jimenez-Munt, M. Marnoni, R. Sabadini, R. Devoti, V. Luceri, C. Ferraro, G. Bianco, Geophysical and geodetic deformation patterns in the Mediterranean, Geophys. Res. Abstracts 4 (27) (2002) EGS02-A-01182.
[22] J. Braun, Three-dimensional numerical simulations of crustal-scale wrenching using a non-linear failure criterion, J. Struct. Geol. 16 (1994) 1173–1186.
[23] J. Chéry, M.D. Zoback, R. Hassani, An integrated mechanical model of the San Andreas Fault in central and northern California, J. Geophys. Res. 106 (2001) 22051–22066.
[24] J.C. Lynch, M.A. Richards, Finite element models of stress orientations in well-developed strike-slip fault zones: Implications for the distribution of lower crustal strain, J. Geophys. Res. 106 (2001) 26707–26729.
[25] J.-C. Bremaecker, P. Hucon, X. LePichon, The deformation of Aegean: a finite element study, Tectonophysics 86 (1982) 197–221.
[26] P.T. Meijer, M.J.R. Wortel, Temporal variation in the stress field of the Aegean region, Geophys. Res. Lett. 23 (1996) 439–442.
[27] P. Lundgren, D. Giardini, R. Russo, A geodynamic framework for eastern Mediterranean kinematics, Geophys. Res. Lett. 25 (1998) 4007–4010.
[28] K.E. Kasapoglu, M.N. Toksoz, Tectonic consequences of the collision of the Arabian and Eurasian plates: finite element models, Tectonophysics 100 (1983) 71–95.
[29] S. Cianetti, P. Gasperini, M. Boccaletti, C. Giunchi, Reproducing the velocity and stress fields in the Aegean region, Geophys. Res. Lett. 24 (1997) 2087–2090.
[30] S. Cianetti, P. Gasperini, C. Giunchi, E. Boschi, Numerical modelling of the Aegean-Anatolian region: geodynamical constraints from observed rheological heterogeneities, Geophys. J. Int. 146 (2001) 760–780.
[31] P. Briole, A. Rigo, H. Lyon-Caen, J.C. Ruegg, K. Papazissi, C. Mitsakaki, A. Balodimou, G. Veis, D. Hatzfeld, A. Deschamps, Active deformation of the Corinth rift, Greece: Results from repeated Global Positioning System surveys between 1990 and 1995, J. Geophys. Res. 105 (2000) 25605–25625.
[32] W.R. Thatcher, Microplate versus continuum descriptions of active tectonic deformation, J. Geophys. Res. 100 (1995) 3885–3894.
[33] Y. Leroy, M. Ortiz, Finite element analysis of strain localization in frictional materials, Int. J. Numer. Anal. Methods Geomech. 13 (1989) 53–74.
[34] P.A. Cundall, M. Board, A microcomputer program for modelling large-strain plasticity problems, in: G. Swoboda (Ed.), International Conference on Numerical Methods in Geomechanics, A.A. Balkema, Brookfield, VT, 1988, pp. 2101–2108.
[35] M.D. Zoback, M.L. Zoback, V.S. Mount, J. Suppe, J.P. Eaton, J.H. Healy, D. Oppenheimer, P. Reasenberg, L.M. Jones, B.C. Raleigh, I.G. Wong, O. Scotti, C. Wentworth, New evidence on the state of stress of the San Andreas fault system, Science 238 (1987) 1105–1111.
[36] W. Thatcher, Present-day crustal movements and the mechanics of cyclic deformation, in: R.E. Wallace (Ed.), The San Andreas Fault system, California, Geological Survey Professional Paper 1515, Washington, DC, 1990, pp. 189–205.
[37] V.S. Mount, J. Suppe, State of stress near the San Andreas fault: Implications for wrench tectonics, Geology 15 (1987) 1143–1146.
[38] L. Fleitout, C. Froidevaux, Tectonics and topography for a lithosphere containing density heterogeneities, Tectonics 1 (1982) 21–56.
[39] J.F. Dewey, Extensional collapse of orogens, Tectonics 7 (1988) 1123–1139.
[40] S. Willet, C. Beaumont, P. Fullsack, Mechanical model for the tectonics of doubly vergent compressional orogens, Geology 21 (1993) 371–374.
[41] C. Straud, H.-G. Kahle, C. Schindler, GPS and geological estimates of tectonic activity in the Marmara Sea region, NW Anatolia, J. Geophys. Res. 102 (1997) 27,587–27,601.
[42] B.J. Meade, B.H. Hager, S.C. Mcclusky, R.E. Reilinger, S. Ergintav, O. Lenk, A.A. Barka, H. Ozener, Estimates of seismic potential in the Marmara Sea region from block models of secular deformation constrained by Global Positioning System measurements, Bull. Seismol. Soc. Am. 92 (2002) 208–215.
[43] I. Jimenez-Munt, R. Sabadini, The block-like behavior of Anatolia envisaged in the modeled and geodetic strain rates, J. Geophys. Res. 29, in press.
[44] J. Chéry, S. Merkel, S. Bouisson, A physical basis for time clustering of large earthquakes, Bull. Seismol. Soc. Am. 91 (2001) 1685–1693.
[45] E. Mantovani, M. Viti, N. Cenni, D. Albarello, D. Babbucci, Short and long term deformation patterns in the Aegean-Anatolian systems: insights from space geodetic data (GPS), Geophys. Res. Lett. 28 (2001) 2325–2328.
[46] E.H. Hearn, B.H. Hager, R. Reilinger, Viscoelastic deformation from North Anatolian fault zone earthquakes and the eastern Mediterranean GPS velocity field, Geophys. Res. Lett. 29 (2002) 1549.

[47] F. Flerit, R. Armijo, G. King, B. Meyer, A.A. Barka, Slip partitioning in the Sea of Marmara pull-apart determined from GPS velocity vectors, Geophys. J. Int. (2002), submitted.
[48] J. Jackson, D. McKenzie, Active tectonics of the Alpine-Himalayan belt between Turkey and Pakistan, Geophys. J. R. Astron. Soc. 77 (1984) 185–264.
[49] O. Alptekin, J.L. Nabeleck, M.N. Toksoz, Source mechanism of the Bartin earthquake of September 3, 1968 in Northwestern Turkey: Evidence for active thrust faulting at the southern Black sea margin, Tectonophysics 122 (1986) 73–88.
[50] A. Zanchi, J. Angelier, Seismotectonics of western Anatolia: regional stress orientation from geophysical and geological data, Tectonophysics 222 (1993) 259–274.
[51] B. Müller, M.L. Zoback, K. Fuchs, L. Mastin, S. Gregersen, N. Pavoni, O. Stephansson, C. Ljunggren, Regional pattern of tectonic stress in Europe, J. Geophys. Res. 97 (1992) 11783–11803.
[52] A.-S. Provost, H. Houston, Orientation of the stress field surrounding the creeping section of the San Andreas fault: Evidence for a narrow mechanically-weak fault zone, J. Geophys. Res. 106 (2001) 11373–11386.